Bull. Mater. Sci. (2019) 42:169
https://doi.org/10.1007/s12034-019-1837-x

A study of electromagnetic light propagation in a perovskite-based solar cell *via* a computational modelling approach

M N SHAIKH[1], Q ZAFAR[2,*] and A PAPADAKIS[3]
[1]Department of Electrical and Computer Engineering, COMSATS University Islamabad, Abottabad 22060, Pakistan
[2]Department of Physics, School of Science, University of Management and Technology, Lahore 54000, Pakistan
[3]Department of Electrical Engineering, School of Engineering, Frederick University, 1036 Nicosia, Cyprus
*Author for correspondence (qayyumzafar@gmail.com)

MS received 1 November 2018; accepted 20 December 2018; published online 23 May 2019

Abstract. Recently, there has been huge surge of scientific interest in organic–inorganic hybrid perovskite solar cells by virtue of their high efficiency and low cost fabrication procedures. Herein, we examine the light propagation inside a planar perovskite solar cell structure (ITO/TiO_2/ZnO/$CH_3NH_3PbI_3$/Spiro-OMeTAD/Al) by solving the Helmholtz equation in the finite element-frequency domain. The simulations were conducted using the COMSOL multiphysics finite element solver to carry out the two-dimensional optical modelling of simulated solar cells in the visible region. It has been observed that shorter wavelengths of light are significantly absorbed by the top region of the photoactive perovskite layer. Specifically, at a wavelength of 400 nm, the effective optical power penetration decays to zero at only 40% of the overall length of the photoactive layer. This observation has been attributed to the high absorption coefficient of the $CH_3NH_3PbI_3$ perovskite material at shorter wavelengths. However, at longer wavelengths, the incident light propagates deeper into the photoactive layer, reaching 100% penetration. Based on the numerical computation, a maximum generation rate of $\sim 3.43 \times 10^{23}$ $m^3 s^{-1}$ has been observed in the photoactive layer at a wavelength of 550 nm.

Keywords. Optical simulation; finite element-frequency domain (FE-FD); Helmholtz equation; organic–inorganic hybrid perovskite; electromagnetic light propagation.

1. Introduction

Solar cells can effectively provide a virtually unlimited amount of clean renewable energy by harvesting sunlight into electrical power [1–3]. Recently, organometallic halide perovskite materials ($CH_3NH_3PbX_3$, X = I, Br and Cl) have offered the promise of a breakthrough in the fabrication of next-generation solar cell devices [4–6]. These photoactive materials have attracted increasing attention due to their high charge carrier mobilities, high extinction coefficient, tuneable optical properties, ambipolar charge transport and significantly long electron–hole diffusion lengths [7–10]. Furthermore, these organic–inorganic hybrid perovskite materials are also compatible with facile, thermal budget and eco-benign fabrication techniques [8,11]. Kumar *et al* [12] have previously confirmed that the fabrication of organic–inorganic perovskite solar cells is easy and cost-effective compared to the conventional Si-based solar cells. Based on these aforementioned unique properties and intensive worldwide cumulative R&D efforts, the power conversion efficiencies (PCE) of perovskite solar cells have skyrocketed from 3 to 23%, within a time-frame of 6 years [13–15].

To further improve the PCE of perovskite solar cells, several reviews thoroughly describe that material design, novel device architectures and efficient light trapping are among future viable pathways [14–16]. In particular, from the optical point of view, it is well understood that broadband absorption enhancement over the whole solar spectrum in perovskite solar cell devices may directly lead to lower recombination currents, higher open-circuit voltages and eventually higher PCE [17]. Therefore, to substantially increase the PCE of the solar cells, there exists a dire need to intensively investigate the optical properties of the photoactive perovskite materials. In this regard, the modelling of solar cells is as important as the experimental work since it allows the optimization of the optical design of solar cell devices and to understand the underlying physics of their operation [18].

Traditionally, to study the light propagation in bulk silicon solar cells, ray-tracing techniques have been widely utilized [19] and are based on the classical laws of geometrical optics. For instance, Brendel [20] studied light coupling into mechanically textured, encapsulated bulk silicon solar cells (thickness of $\sim$250 μm) by 3-D ray tracing using the SUNRAYS software package. However, it is noteworthy that this technique may only be used whenever the geometrical size of the photoactive layer is much larger than the optical wavelength. For thin film solar cells, where the film thickness becomes comparable or smaller than the wavelength of light [21], light propagation cannot be adequately modelled by ray tracing and instead it is necessary to rigorously solve Maxwell's

equations [22–24]. Therefore, numerical simulations capable of solving the Maxwell's equations and semiconductor equations (Poisson, continuity and drift-diffusion equations) are routinely performed to develop an understanding regarding the optoelectronic properties of solar cells [25,26]. Miyazaki *et al* [27] have investigated a hydrogenated amorphous silicon (a-Si:H) solar cell theoretically based on current continuity and Poisson equations.

Currently, there have been a number of numerical methods capable of simulating wave propagation in solar cell devices, such as the finite difference [28], finite volume [29] and finite element methods [30]. In the present study, we have simulated the light propagation through solar cells by utilizing a powerful computational technique, the solution of the Helmholtz equation in the finite element-frequency domain (FE-FD). In general, the finite element method is used to model discontinuities in light propagation in realistic, arbitrary, complex and non-uniform geometries, more accurately and efficiently as compared to finite difference and finite volume methods [31].

The objective of the present study is to numerically compute the electromagnetic field distribution in various layers of perovskite-based solar cells (ITO/TiO_2/ZnO/$CH_3NH_3PbI_3$/Spiro-OMeTAD/Al) in the visible region (wavelength of 400–700 nm) of incident light. We intend to establish a multiphysics framework to obtain insight pertaining to light propagation, absorption and charge carrier's generation in the photoactive layer. The present optical model self-consistently solves the partial differential equation (i.e., Helmholtz equation) using the FE-FD method and allows for composition dependent material parameters. Herein, we are motivated to examine methylammonium lead iodide ($CH_3NH_3PbI_3$) as the photoactive perovskite layer by virtue of its interesting optoelectronic properties [32]. It is a semiconducting pigment with the direct band gap, $E_g = 1.55$ eV that allows efficient light absorption over the whole visible spectrum [33]. Furthermore, the excitons produced by light absorption in $CH_3NH_3PbI_3$ have a weak binding energy of about 0.030 eV [34], thereby allowing rapid dissociation of excitons into free charge carriers at room temperature.

2. Numerical modelling approach

The schematic cross-section of the simulated perovskite-based solar cell is depicted in figure 1a. The simulated solar cell (from top to bottom) consists of an indium tin oxide (ITO) transparent front contact (80 nm) deposited on the thin glass substrate (150 nm). The ITO thin film is followed by 120 and 150 nm thin electron transport layers of TiO_2 and ZnO, respectively. The photoactive layer consists of 500 nm thin methylammonium lead iodide ($CH_3NH_3PbI_3$) perovskite layer. A 100 nm hole transport layer of 2,2′-,7,7′-Tetrakis[*N*,*N*-di(4-methoxyphenyl)amino]-9,9-spirobifluorene (Spiro-OMeTAD) and aluminium metal back contacts have been utilized. The layer stack of the solar cell is in agreement with solar cell structures used in the literature [35–37]. In the present study, we have numerically modelled the ITO/TiO_2/ZnO/$CH_3NH_3PbI_3$/Spiro-OMeTAD/Al planar structure to study the optical wave propagation within the layer stack of the simulated solar cell. Generally, the incident optical power is quantified by the standard spectral irradiance distribution curve (i.e., spectral irradiance as a function of wavelengths of incident photons). Herein, all FE-FD optical, simulations have been carried out in two-dimensions (2D) for selected wavelengths ranging from 400 to 700 nm. The solar irradiance at AM-1.5 for the selected wavelengths is depicted in figure 1b.

The transverse electromagnetic light impinging on the solar cell is normally divided into two polarization modes, the transverse electric (TE) and transverse magnetic (TM) [28]. Typically, when the electric field is perpendicular to the plane of incidence, then, it is associated with the TE mode. In contrast, when the electric field is in parallel with the plane of incidence, then, it is associated with the TM mode. In the case of TEM mode, however, both electric and magnetic fields are perpendicular to the plane of incidence. In the present numerical simulation, the calculations for electric field intensity of the incident light wave have been carried out using the well-established Helmholtz equation [38], depicted as equation (1):

$$\nabla \times (\nabla \times E) - k_o^2 \varepsilon_r E = 0, \tag{1}$$

where k_o is the wave vector of the incident light, ε_r the dielectric permittivity of the medium which is related to the complex refractive index $(n + ik)$ of photoactive materials. Therefore, the optical dispersion *n*–*k* curves (as a function of wavelength) play a key role in carrying out an accurate optical simulation. Here, the optical constants (n and k) of each layer (x, y and z) have been adapted from the literature [39–43], and used as input parameters in our simulator. The real part of the refractive index $n(\lambda)$ and extinction coefficient $k(\lambda)$ used in our study are depicted in figure 2a and b, respectively, as a function of selected wavelengths.

In the optical approach of simulations, the effects of light reflection, transmission and absorption in every layer have been considered prior to light harvesting by the photoactive perovskite layer. It is well-understood that the wavelength dependent dielectric permittivity function defines the capacity of a material to absorb, reflect and transmit incident light [44]. Therefore, electromagnetic field's reflection (R) and transmission (T) coefficients have been facilely computed by the Fresnel equations, since the optical properties $n(\lambda)$ and $k(\lambda)$ of the constituent layers in solar cells are already known (figure 2a and b). In this way, multiple diffusion of light inside the solar cell structure has been taken into consideration successfully. The optical power absorption inside the solar cell structure has been estimated using equation (2), as follows [45]:

$$P(x) = (1 - R) P_o \exp(-\alpha x), \tag{2}$$

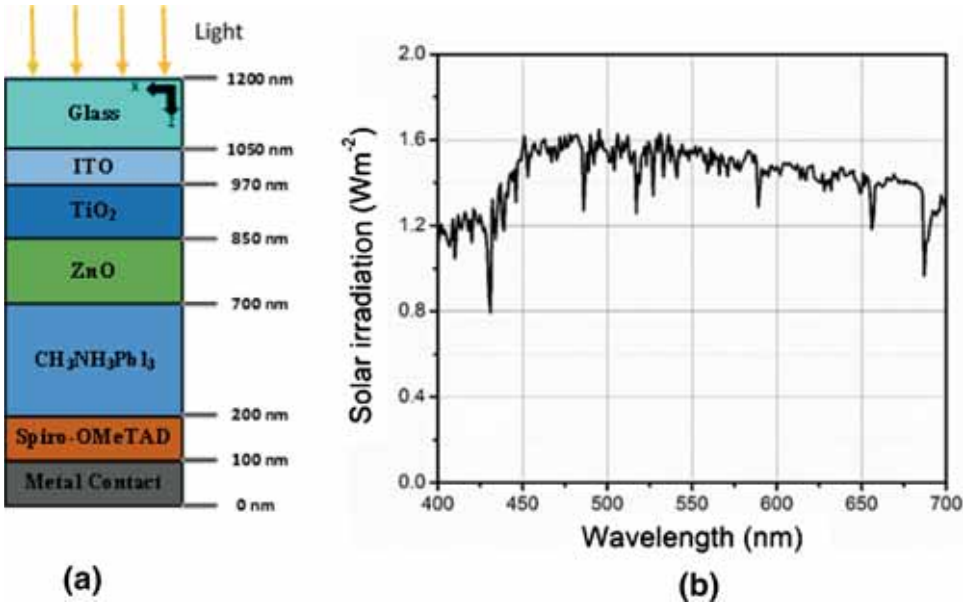

Figure 1. (**a**) Simulated perovskite-based solar cell structure and (**b**) selected wavelength solar irradiance at AM-1.5.

where $P(x)$ represents the optical power at any position x inside the solar cell structure, whereas P_o represents the incident optical power. The term α represents the absorption coefficient and it is related to the extinction coefficient by the mathematical expression $\alpha = 4\pi k/\lambda$ [46]. The results of the absorption coefficient of various layers in solar cells as a function of $k(\lambda)$ are shown in figure 3.

The light impinging on the solar cell induces charge carrier generation in the photoactive layer of the cell structure by the absorption of photons [47–49]. The charge carrier generation is directly related to this internal power flux by the following relation [45]:

$$G(x) = \frac{\alpha\lambda P(x)}{hc}, \tag{3}$$

where c and h represent the speed of light and Plank's constant, respectively. The term G indicates charge carriers' generation rate at any position x for a specific wavelength λ of the incident light. Since, the generation rate is the number of carriers produced per second per volume inside the device, therefore, a final integration over the selected wavelength range has been performed to culminate total charge carrier generation inside the solar cell. It has been mathematically expressed by the following relation:

$$G_{\text{eff}} = \int_{400\,\text{nm}}^{700\,\text{nm}} G(x,\lambda)d\lambda. \tag{4}$$

The photon flux N is related to the incident optical power flux P_o as described below:

$$P_o = NqE_p, \tag{5}$$

where q and E_p represent the electronic charge and energy per incident photon in *Ev*, respectively.

In optical simulations, apart from spectral irradiance, the photon flux (N) is also required to calculate the internal quantum efficiency η as a number of produced carriers per incident photons.

$$\eta = G/N. \tag{6}$$

3. Results and discussion

To examine the optical behaviour of perovskite solar cells, electromagnetic analysis has been performed using the FE-FD method. Visible-wavelength transverse electromagnetic light has been injected at normal incidence to the perovskite solar cell structure to quantify the expected light absorption by the photoactive layer. Using the Helmholtz equation (equation (1)), the electric field (E) inside the perovskite solar cell has been computed using COMSOL Multiphysics software at five different wavelengths within the visible region. It can be observed from the 1-D electric field distribution (depicted in figure 4) that at shorter wavelengths, the electric field attenuates significantly inside the photoactive layer. This phenomenon is observed because light is strongly absorbed by the perovskite layer due to the significantly higher absorption coefficient of $CH_3NH_3PbI_3$ at a wavelength of 400 nm (as previously shown in figure 3). However, as the light wavelength increases, weak absorption in $CH_3NH_3PbI_3$ causes a slow decaying rate of the electric field intensity. This results in comparatively higher electric field distribution within the photoactive film. In the present FE-FD electromagnetic analysis, the cross-sectional profile for the electric field intensity has

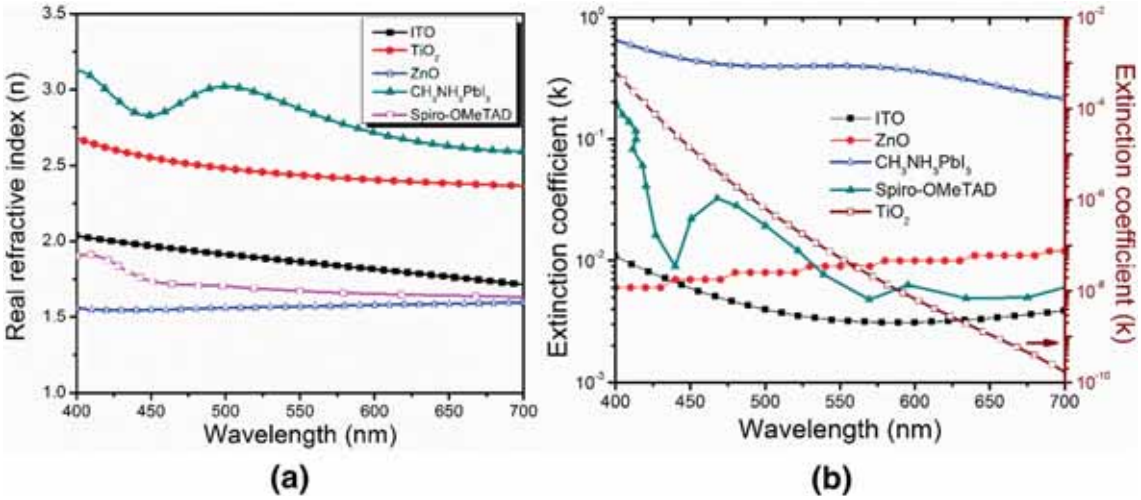

Figure 2. (**a**) Real component of the refractive index and (**b**) extinction coefficient, as a function of selected wavelengths.

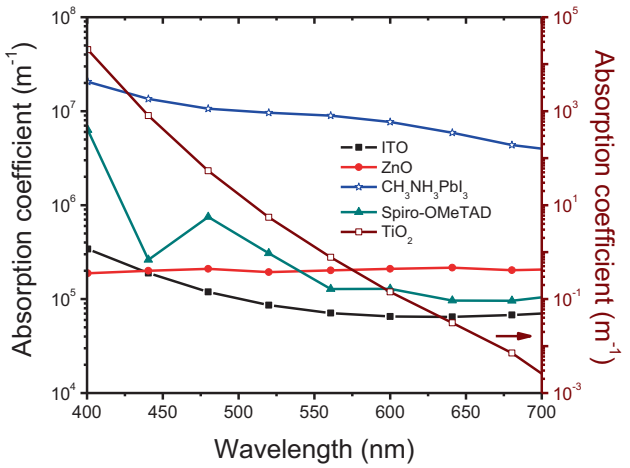

Figure 3. Absorption coefficient of constituent layers of the simulated solar cell at the selected wavelength range.

also been investigated in the x–z plane of the solar cell. The 2D profile is depicted in figure 4 (inset: a and b) and describes the electric field intensity distribution at wavelengths of 400 and 700 nm, respectively. It can be clearly shown that the electric field inside the photoactive layer is relatively stronger at incident light with a wavelength of 700 nm as compared to the wavelength of 400 nm. It is pertinent to mention that in the present study, the visible wavelength range has been used since the optical properties for perovskite solar cells are only currently available within the visible wavelength region. However, the developed simulator can also be applied for the broadband such as the UV–Vis–IR range as well, given that optoelectronic properties for the materials at these wavelengths are available from the literature.

In the present simulated solar cell, the incident light has to propagate first through the top transparent electrode and then through the n-type layers before reaching the photoactive $CH_3NH_3PbI_3$ layer. As a consequence, assessing the optical propagation and losses within the solar cell structure is a critical issue. Using the FE-FD analysis, we have calculated the absorbed optical power inside the solar cell's structure based on equation (2). Since the horizontal line in figure 5 represents the vertical length of the simulated solar cell, it can be clearly observed that most of the incident energy first propagates downwardly along the z-direction before it is totally absorbed in the photoactive layer. Furthermore, it can also be observed from 1-D analysis (depicted in figure 5) that the optical power penetrates more deeply in the perovskite solar cell for longer wavelengths as compared to shorter wavelengths. Specifically, at a wavelength of 400 nm, the effective optical power penetrates only to 40% of the overall length of the photoactive layer, whereas for 700 nm, the significant optical power penetrates to nearly 100%. From the cross-section of 2-D optical profile analysis (depicted in figure 5, inset: a and b), it can be clearly observed that for a light wavelength of 700 nm, nearly the whole photon flux is trapped within the photoactive layer, indicating that the optical power absorption in the photoactive layer is significantly higher at shorter wavelength (400 nm).

Figure 6 shows the 1-D charge carrier generation profiles within the layer stack of the simulated solar cell for the normal incident light with wavelengths of 400, 475, 550, 625 and 700 nm. Figure 6 shows that the contribution of charge carrier generation in the photoactive perovskite layer is considerably higher. This observation is reasonable since typically front contact, back metal contact, p-layer and n-layer do not contribute significantly to the charge carrier generation [23]. Furthermore, as previously observed in figures 4 and 5, at short wavelengths, the electric field and absorbed optical power exhibit significantly small magnitudes in the bottom region of the perovskite layer, which shows that mostly the charge carriers are generated in the top region of the

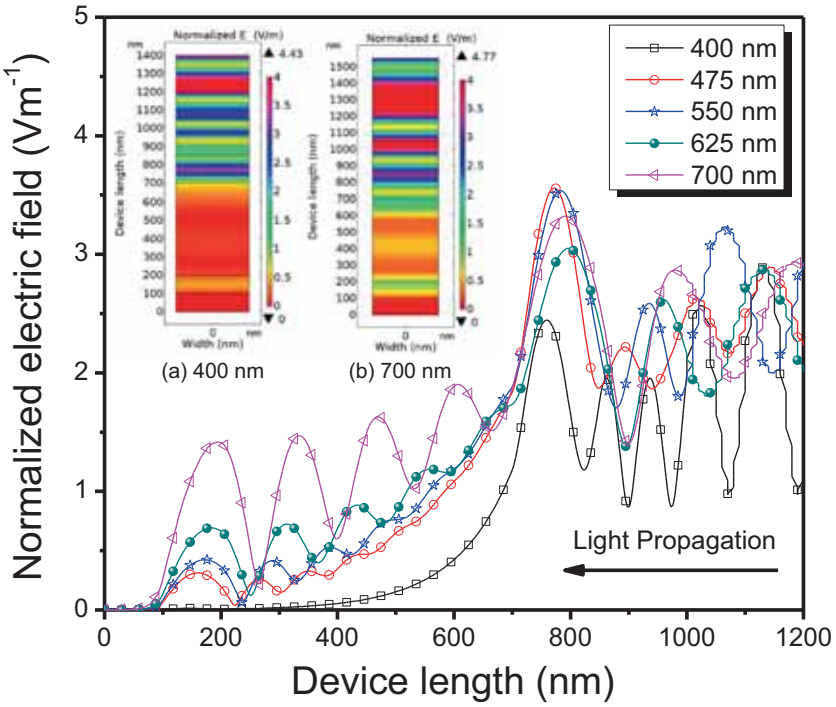

Figure 4. 1-D and (inset) 2-D cross-sectional normalized electric field distributions inside the layer stack of the simulated solar cell at varied incident wavelengths.

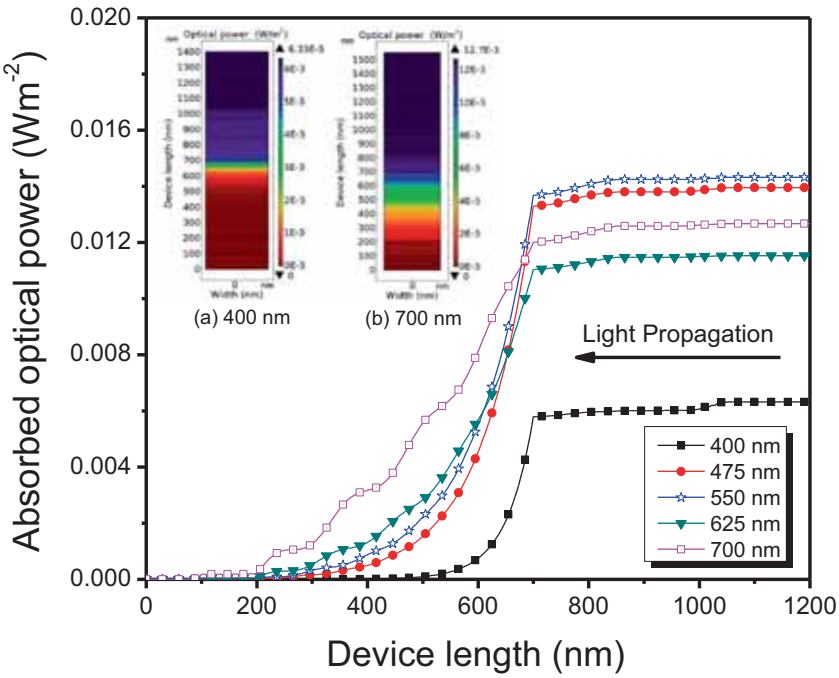

Figure 5. 1-D and (inset) 2-D cross-sectional absorbed optical power distributions inside the layer stack of the simulated solar cell at varied incident wavelengths.

photoactive layer. However, as the wavelength increases, the electric field intensity at the bottom of the perovskite layer also strengthens which leads to the charge carriers appearing in the whole region of the photoactive layer. A maximum generation rate of $3.43 \times 10^{23}\,m^3\,s^{-1}$ has been observed in the $CH_3NH_3PbI_3$ photoactive layer at wavelength of

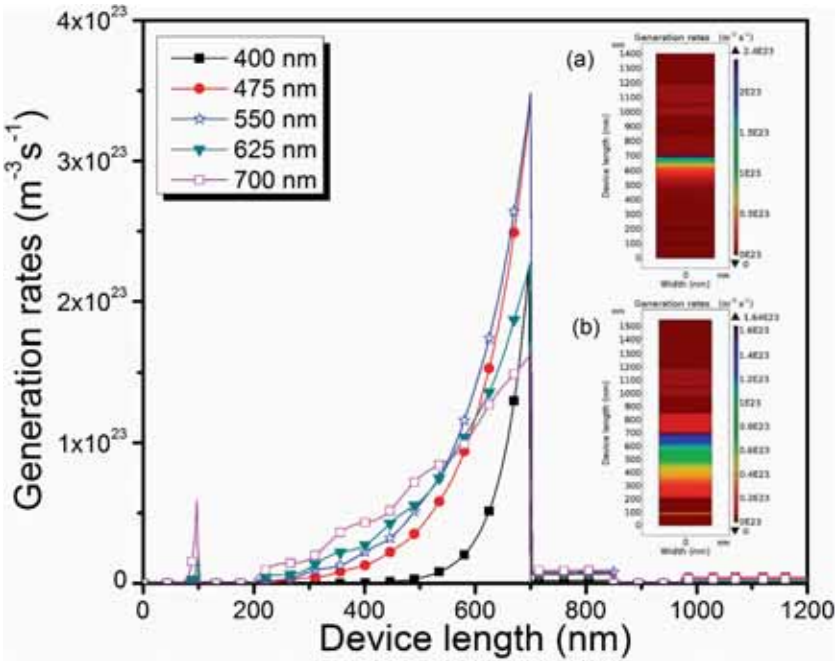

Figure 6. 1-D and (inset) 2-D cross-sectional generation rate profile inside the layer stack of the simulated solar cell at varied incident wavelengths.

550 nm. For comparison purposes, it may be of reader's interest that Rajib *et al* [50] have previously reported a generation rate of the order of 10^{26} in silicon-based PIN solar cells. Figure 6 (inset: a and b) shows the cross-section of 2-D charge carrier generation profile in the perovskite solar cell for the transverse electromagnetic light at 400 and 700 nm, respectively.

4. Conclusion

To summarize, we have developed a multiphysics model for perovskite-based solar cells by solving the Helmholtz equation in the FE-FD. A typical structure of a typical perovskite solar cell is presented together with the corresponding optical constants of its constituent layers. The mathematical model involved in optical modelling of the simulated solar cell is also presented and is capable of analysing light propagation at the nanometre scale. Using this model, we have successfully presented detailed light propagation and absorption profiles (one- and two-dimensional) in each constituent layer of the simulated solar cell ($ITO/TiO_2/ZnO/CH_3NH_3PbCl_3$/Spiro-OMeTAD/Al). From the distribution of the electromagnetic field and absorbed optical power, we have also numerically computed the effective charge generation rate within the photoactive perovskite layer as a function of the photon wavelength ranging from 400–700 nm. The present study emphasizes critical basis and insightful guidelines for the futuristic development of a three-dimensional unified optoelectronic model coupled with a light-trapping scheme to achieve efficient perovskite-based solar cell design and optimization.

Acknowledgements

We are highly grateful to the Erasmus Mundus Intact (EMINTACT) mobility program for providing PhD fellowship for M N Shaikh.

References

[1] Eshaghi A and Aghaei A A 2015 *Bull. Mater. Sci.* **38** 1177
[2] Siwach B, Mohan D, Sharma S and Jyoti D 2017 *Bull. Mater. Sci.* **40** 1371
[3] Alwin S, Ramasubbu V and Shajan X S 2018 *Bull. Mater. Sci.* **41** 27
[4] Rakstys K, Paek S, Gao P *et al* 2017 *J. Mater. Chem. A* **5** 7811
[5] Lin Q, Nagiri R C R, Burn P L and Meredith P 2017 *Adv. Opt. Mater.* **5** 1600819
[6] Hutter E M, Hofman J J, Petrus M L *et al* 2017 *Adv. Energy Mater.* **7** 1602349
[7] Jeon N J, Noh J H, Kim Y C, Yang W S, Ryu S and Seok S I 2014 *Nat. Mater.* **13** 897
[8] Niu G, Guo X and Wang L 2015 *J. Mater. Chem. A* **3** 8970
[9] Green M A, Jiang Y, Soufiani A M and Ho-Baillie A 2015 *J. Phys. Chem. Lett.* **6** 4774
[10] Grätzel M 2017 *Acc. Chem. Res.* **50** 487
[11] Green M A, Ho-Baillie A and Snaith H J 2014 *Nat. Photonics* **8** 506

[12] Kumar M S, Charanadhar N, Srikanth V V, Rao K B S and Raj B 2018 *Bull. Mater. Sci.* **41** 62
[13] Sakai N, Wang Z, Burlakov V M, Lim J, McMeekin D, Pathak S *et al* 2017 *Small* **13** 1602808
[14] Correa-Baena J-P, Abate A, Saliba M, Tress W, Jacobsson T J, Grätzel M *et al* 2017 *Energy Environ. Sci.* **10** 710
[15] Kevin A B, Axel F P, Zhengshan Y, Mathieu B, Rongrong C, Jonathan P M *et al* 2017 *Nat. Energy* **2** 17009
[16] Asghar M, Zhang J, Wang H and Lund P 2017 *Renew. Sustain. Energy Rev.* **77** 131
[17] Han G, Zhang S, Boix P P, Wong L H, Sun L and Lien S-Y 2017 *Prog. Mater. Sci.* **87** 246
[18] Kumar K R and Zeman M 2008 *Bull. Mater. Sci.* **31** 737
[19] Yagi T, Uraoka Y and Fuyuki T 2006 *Sol. Energy Mater. Sol. Cells* **90** 2647
[20] Bierhoff T, Wallrabenstein A, Himmler A, Griese E and Mrozynski G 2001 *IEEE Trans. Magn.* **37** 3307
[21] Rim S-B, Zhao S, Scully S R, McGehee M D and Peumans P 2007 *Appl. Phys. Lett.* **91** 243501
[22] Shaikh M, Acharya P and Papadakis A 2016 *5th International Conference on Renewable Energy Sources & Energy Efficiency—New Challenges*, p 1
[23] Parsons R, Tamang A, Jovanov V, Wagner V and Knipp D 2017 *Appl. Sci.* **7** 427
[24] Semenikhin I, Zanuccoli M, Benzi M, Vyurkov V, Sangiorgi E and Fiegna C 2012 *Opt. Quant. Electron.* **44** 149
[25] Lin Q, Armin A, Nagiri R C R, Burn P L and Meredith P 2015 *Nat. Photonics* **9** 106
[26] Phillips L J, Rashed A M, Treharne R E, Kay J, Yates P, Mitrovic I Z *et al* 2016 *Sol. Energy Mater. Sol. Cells* **147** 327
[27] Miyazaki K, Matsuki N, Shinno H, Fujioka H, Oshima M and Koinuma H 1999 *Bull. Mater. Sci.* **22** 729
[28] Ong K G, Varghese O K, Mor G K, Shankar K and Grimes C A 2007 *Sol. Energy Mater. Sol. Cells* **91** 250
[29] Fell A 2013 *IEEE Trans. Electron. Devices* **60** 733
[30] Isabella O, Solntsev S, Caratelli D and Zeman M 2013 *Prog. Photovolt. Res. Appl.* **21** 94
[31] Thiele E S and French R H 1998 *J. Am. Ceram. Soc.* **81** 469
[32] Ziang X, Shifeng L, Laixiang Q, Shuping P, Wei W, Yu Y *et al* 2015 *Opt. Mater. Express* **5** 29
[33] Choi J J, Yang X, Norman Z M, Billinge S J and Owen J S 2013 *Nano Lett.* **14** 127
[34] Grätzel M 2014 *Nat. Mater.* **13** 838
[35] Hossain M F, Faisal M and Okada H 2016 *2nd International Conference on Electrical, Computer & Telecommunication Engineering (ICECTE)*, p 1
[36] Lin Q, Armin A, Nagiri R C R, Burn P L and Meredith P 2015 *Nat. Photonics* **9** 106
[37] Liu D and Kelly T L 2014 *Nat. Photonics* **8** 133
[38] Lin A and Phillips J 2008 *Sol. Energy Mater. Sol. Cells* **92** 1689
[39] Yu L, Misra S, Wang J, Qian S, Foldyna M, Xu J *et al* 2014 *Sci. Rep.* **4** 4357
[40] Muchuweni E, Sathiaraj T and Nyakotyo H 2017 *Heliyon* **3** e00285
[41] König T A, Ledin P A, Kerszulis J, Mahmoud M A, El-Sayed M A, Reynolds J R *et al* 2014 *ACS Nano* **8** 6182
[42] Filipič M, Löper P, Niesen B, De Wolf S, Krč J, Ballif C *et al* 2015 *Opt. Express* **23** A263
[43] Phillips L J, Rashed A M, Treharne R E, Kay J, Yates P, Mitrovic I Z *et al* 2015 *Data Brief* **5** 926
[44] Gunaicha P P 2012 MS Thesis (Ohio: The University of Toledo)
[45] Sze S M and Ng K K 2006 *Physics of semiconductor devices* (USA: John Wiley & Sons)
[46] Hoppe H, Arnold N, Sariciftci N and Meissner D 2003 *Sol. Energy Mater. Sol. Cells* **80** 105
[47] Malik H A, Aziz F, Asif M, Raza E, Najeeb M A, Ahmad Z *et al* 2016 *J. Lumin.* **180** 209
[48] Zafar Q, Najeeb M A, Ahmad Z and Sulaiman K 2015 *J. Nanopart. Res.* **17** 372
[49] Ahmad Z, Abdullah S M, Zafar Q and Sulaiman K 2014 *J. Mod. Opt.* **61** 1730
[50] Rajib M R, Rana S M, Hasan M R, Amin R, Iqbal M S, Anik M R *et al* 2014 *Int. J. Eng. Res. Technol.* **3** 1